UC Irvine

UC Irvine Previously Published Works

Title

Formation and Clearance of All-Trans-Retinol in Rods Investigated in the Living Primate Eye With Two-Photon Ophthalmoscopy.

Permalink

https://escholarship.org/uc/item/42z559x0

Journal

Investigative Ophthalmology and Visual Science, 58(1)

Authors

Sharma, Robin
Schwarz, Christina
Hunter, Jennifer
et al.

Publication Date

2017

DOI

10.1167/iovs.16-20061

Peer reviewed

eScholarship.org Powered by the California Digital Library
University of California

Formation and Clearance of All-*Trans*-Retinol in Rods Investigated in the Living Primate Eye With Two-Photon Ophthalmoscopy

Robin Sharma,[1] Christina Schwarz,[1] Jennifer J. Hunter,[1–3] Grazyna Palczewska,[4] Krzysztof Palczewski,[5] and David R. Williams[1,2,6]

[1]Center for Visual Science, University of Rochester, Rochester, New York, United States
[2]Flaum Eye Institute, University of Rochester, Rochester, New York, United States
[3]Biomedical Engineering, University of Rochester, Rochester, New York, United States
[4]Polgenix, Inc., Cleveland, Ohio, United States
[5]Department of Pharmacology, Case Western Reserve University, Cleveland, Ohio, United States
[6]The Institute of Optics, University of Rochester, Rochester, New York, United States

Correspondence: Robin Sharma, Center for Visual Science, University of Rochester, 601 Elmwood Avenue, Box 319, Rochester, NY 14620, USA; sharmarobin@gmail.com.

Submitted: June 3, 2016
Accepted: November 17, 2016

Citation: Sharma R, Schwarz C, Hunter JJ, Palczewska G, Palczewski K, Williams DR. Formation and clearance of all-*trans*-retinol in rods investigated in the living primate eye with two-photon ophthalmoscopy. *Invest Ophthalmol Vis Sci*. 2017;58:604–613. DOI:10.1167/iovs.16-20061

Purpose. Two-photon excited fluorescence (TPEF) imaging has potential as a functional tool for tracking visual pigment regeneration in the living eye. Previous studies have shown that all-*trans*-retinol is likely the chief source of time-varying TPEF from photoreceptors. Endogenous TPEF from retinol could provide the specificity desired for tracking the visual cycle. However, in vivo characterization of native retinol kinetics is complicated by visual stimulation from the imaging beam. We have developed an imaging scheme for overcoming these challenges and monitored the formation and clearance of retinol.

Methods. Three macaques were imaged by using an in vivo two-photon ophthalmoscope. Endogenous TPEF was excited at 730 nm and recorded through the eye's pupil for more than 90 seconds. Two-photon excited fluorescence increased with onset of light and plateaued within 40 seconds, at which point, brief incremental stimuli were delivered at 561 nm. The responses of rods to stimulation were analyzed by using first-order kinetics.

Results. Two-photon excited fluorescence resulting from retinol production corresponded to the fraction of rhodopsin bleached. The photosensitivity of rhodopsin was estimated to be 6.88 ± 5.50 log scotopic troland. The rate of retinol clearance depended on intensity of incremental stimulation. Clearance was faster for stronger stimuli and time constants ranged from 50 to 300 seconds.

Conclusions. This study demonstrates a method for rapidly measuring the rate of clearance of retinol in vivo. Moreover, TPEF generated due to retinol can be used as a measure of rhodopsin depletion, similar to densitometry. This enhances the utility of two-photon ophthalmoscopy as a technique for evaluating the visual cycle in the living eye.

Keywords: ophthalmic imaging, photoreceptors, visual cycle, pigment regeneration

Retinal degenerations that affect the outer retina can disrupt the normal function of photoreceptors and RPE. To maintain visual pigments in the preactivated state, substantial trafficking of retinoid molecules[1–3] takes place between the RPE and photoreceptors. Disruptions of this flow can have varying consequences that lead to pathologies such as retinitis pigmentosa, Stargardt disease, Leber congenital amaurosis, or AMD.[3–5] Diagnoses of the onset of any type of outer retinal degeneration rely on robust and noninvasive detection of anomalies in the physiology of photoreceptor-RPE interactions with high sensitivity and specificity. Visual pigment regeneration is a biochemical process crucial for sustaining vision, and measurement of its kinetics is a valuable indicator of the health of the photoreceptor and RPE layers.[6] Rhodopsin densitometry has previously been used to approximate relative pigment density to estimate the photosensitivity of rhodopsin[7–10] and measure the kinetics of pigment regeneration.[10–12] Such time-consuming studies require complete dark adaptation and often are unreliable.[13,14] Better methods are needed to overcome these shortcomings and objectively, rapidly, and safely probe the visual cycle.

Two-photon excitation[15] is a suitable technique for tracking specific steps of the visual cycle. Studies in wild-type and knockout mice have previously demonstrated that two-photon excited fluorescence (TPEF) imaging can visualize endogenous fluorophores, such as retinol, retinyl esters, and retinoid condensation products in the RPE.[16–18] Moreover, two-photon imaging in mice has also been used to study progression of visual cycle defects with age[18,19] and identify promising candidates for drug development.[20] Although rodents are invaluable animal models that have yielded important insights into the chemistry of the healthy and defective visual cycle,[3,21] their retinas are different and visual cycle kinetics are much slower than humans.[6] For developing novel ophthalmic imaging techniques that can eventually be used in the clinic, nonhuman primates are the ideal gateway animal model

This work is licensed under a Creative Commons Attribution-NonCommercial-NoDerivatives 4.0 International License.

Investigative Ophthalmology & Visual Science

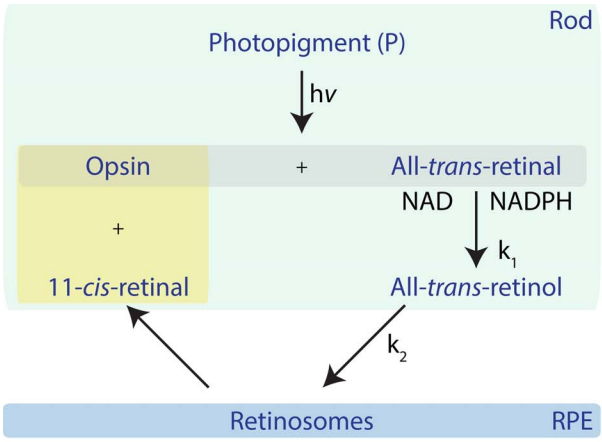

(a)

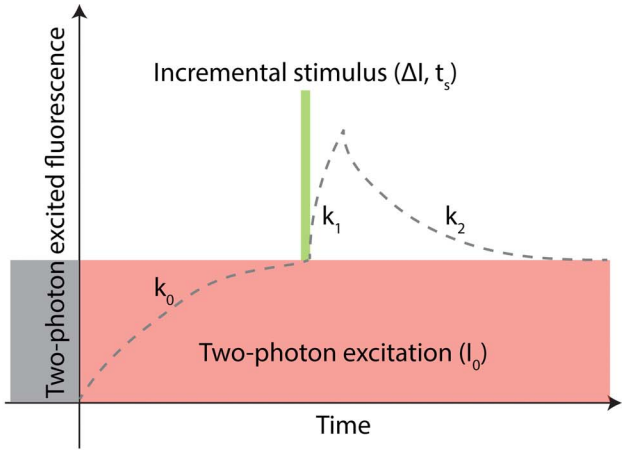

(b)

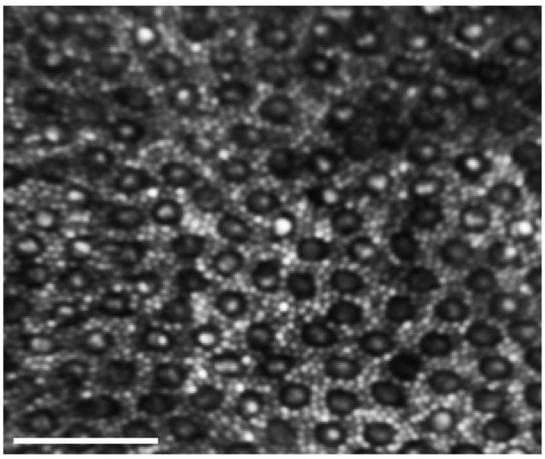

(c)

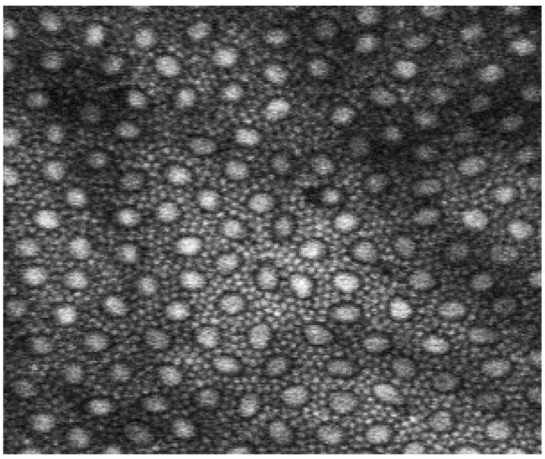

(d)

Figure 1. (**a**, **b**) Schematic representation of the visual cycle and measured kinetic phases of formation and clearance of endogenous fluorescence derived from retinol. (**a**) The visual cycle is simplified for clarity to show only selected retinoids. (**b**) Schematic of the imaging protocol. The *gray band* before imaging represents the period of dark adaptation when no stimulus is present. With the onset of imaging, steady stimulation from the two-photon excitation light source is shown in *dark pink* and labeled as I_0, and a brief incremental stimulus is in *light green*. Here, k_0 refers to the time constant for the single-exponential fit to the time course of TPEF before the delivery to the stimulus (shown in *light green*), whereas k_1 and k_2 are as defined in (**a**). The *dashed curve* in (**b**) illustrates qualitatively the TPEF time course and is not representative of actual data. Representative images of the photoreceptor mosaic are shown in (**c**) and (**d**). The image in (**c**) is a reflectance image captured through the TPF-AOSLO in confocal mode through a pinhole conjugate to the retina. The image in (**d**) is a time-averaged TPEF image of the same cells. Rods and cones are visible in both images. *Scale bar*: 50 μm. NAD, nicotinamide adenine dinucleotide; NADH, reduced form of NAD.

because their retinal architecture is similar to humans.[22] Adaptive optics–assisted TPEF imaging of endogenous fluorophores of the inner and outer retina has been previously demonstrated in the living primate eye.[23] Although TPEF can be captured from multiple retinal layers, two-photon imaging of photoreceptors is of major interest because photoreceptor fluorescence varies with time after light exposure[24,25] and may provide a valuable measure of outer retinal health.

All-*trans*-retinol is an intermediate component of the visual cycle. It is formed after reduction of all-*trans*-retinal within photoreceptor outer segments and in rods it is cleared to the RPE thereafter (schematic shown in Fig. 1a). It is likely to be the most dominant endogenous source of time-varying fluorescence within photoreceptors when TPEF is excited at 720 to 730 nm.[24,26–28] Even though we have been able to track TPEF over time, it has been challenging to directly estimate and quantify mechanistic aspects of retinol formation, as well as retinol clearance because of the inadvertent stimulation of the retina by the imaging light source.[24,29] Previously, this problem was overcome by using an imaging protocol that necessitated the acquisition of multiple videos of 2 minutes' duration from the same retinal location after varying periods of dark adaptation requiring several hours.[24] This practice is time-consuming and prone to variability, demanding an improved protocol for rapidly and reliably measuring retinol kinetics using in vivo two-photon imaging.

The goal of this work was to develop and deploy an experimental and analytical scheme for rapid quantification of retinol formation and clearance in the living eye using two-photon ophthalmoscopy. Here we have used this framework to quantify some crucial aspects of all-*trans*-retinol physiology in rod photoreceptors in nonhuman primates.

Methods

Animal Preparation

Three *Macaca fascicularis* were used in this study (one female, 6 years old, and two males, 6 and 9 years old).

Investigative Ophthalmology & Visual Science

Table. List of Light Sources, Their Wavelengths, and Their Respective Intensities Incident on the Retina During Imaging, as Described in Figure 1a

Light Sources	Wavelength, nm	Power Incident at Pupil	Range of Exposure Duration, s
Two-photon excitation, I_0	730	3.5 mW	75–100
Visible stimulus, ΔI	561	32–123 μW	0.07–0.38
Wavefront sensing beacon	840	<50 μW	Always on

Procedures for handling these subjects were approved by the University of Rochester's committee for animal research. Before each experiment, ketamine (10–20 mg/kg) and valium (0.25 mL/kg) were used for sedating the animals. Soon after, they were intubated and kept anesthetized for several hours with isoflurane (ranging from 1%–5%). Only one eye was imaged at a time. A speculum was used to keep the eye open during the experiment and a contact lens appropriate to the corneal curvature was used to minimize lower-order ocular aberrations. A hydrating gel (Genteal; Alcon, Fort Worth, TX, USA) was applied between the eye and the contact lens to maintain hydration and optical quality of the cornea. To reduce involuntary eye-drifts, animals were paralyzed with vecuronium (60 μg/kg/h) for up to 6 hours, and during paralysis, their breathing was maintained by a ventilator. Animals were placed on a motorized stereotaxic cart during imaging with their eye located at the cart's gimbal point, and light was steered to different retinal locations by moving the animal's body about the gimbal point, in a manner described previously.[24]

Two-Photon Fluorescence Adaptive Optics Scanning Light Ophthalmoscope (TPF-AOSLO)

All experiments were conducted with a custom TPF-AOSLO. In brief, an adaptive optics (AO) subsystem measured and corrected the wavefront aberration of the eye's optics.[30,31] In conjunction, ultrashort pulses of approximately 55 fs pulse-width tuned to a center wavelength of 730 nm emitted at a repetition rate of 80 MHz from a pulsed light source (Mai Tai XF-1; Spectra Physics, Newport, Irvine, CA, USA) were directed at the pupil of the eye and shared a common beam path with the AO subsystem. After AO correction, minimally aberrated light from the Mai Tai laser was focused for imaging photoreceptors through the optics of the eye. Light was raster scanned across the retina at 26.7 Hz frame rate over a 1.3 × 1.1 degree field of view. Videos were simultaneously recorded from two different detection channels. Pulsed light used for two-photon excitation generated autofluorescence that was captured in single-pass (without descanning) by a photomultiplier tube (PMT) sensitive to visible light. Light from the same source and backscattered from the retina was detected in double pass through a confocal pinhole by a PMT sensitive to near-infrared light. This channel was used both to estimate the interframe retinal motion within both videos due to heart rate and breathing artifacts and to generate registered videos.[32] Data were recorded at 35 MHz pixel clock in both channels. Details of this apparatus have been described previously,[24] although minor modifications were made for this study as follows:

1. An additional light source was used for visible stimulation (iChrome MLE-L; Toptica Photonics, Inc., Victor, NY, USA). Light from the Toptica laser propagated through the entire AOSLO before being delivered to the eye. It was focused at the photoreceptor layer and scanned across the retina with the imaging beam.[33,34] The wavelength used for stimulation was 561 nm for all experiments reported here.
2. The dichroic used for collecting the emitted two-photon fluorescence was chosen to permit the transmission of light at 561 nm (T545LPXRXT; Chroma Technology Corp., Bellows Falls, VT, USA) into the PMT.
3. Two sets of two barrier filters (E550SP-2p and ET680SP-2P8; Chroma Technology Corp.) were placed in front of the PMT to prevent bleed-through of light from the visible stimulus at 561 nm. Consequently, effective emission collection was limited to the 400–500 nm spectral bands.

Imaging Protocol

A schematic of the experimental implementation is shown in Figure 1b. After a sufficient period of constant illumination by the two-photon excitation source, TPEF reaches a plateau value, likely due to the achievement of an equilibrium between retinol formation and clearance.[24] An analytical framework has been developed to estimate the concentration of retinol under steady-state illumination (see Appendix). Based on the insight gained by this simplistic analytical model, a modified imaging scheme has been developed, in which an incremental stimulus is delivered to the retina during the steady-state phase after equilibrium has been achieved. The magnitude of duration of the incremental stimulus can considerably influence the analysis and interpretation of data. Calculations described in the Appendix show that if the temporal duration of the incremental stimulus is very short (akin to an ideal delta function), then the kinetic parameters of retinol formation and clearance can be directly extracted from the subsequent impulse response by fitting a double exponential function.

Before imaging, the retina was dark adapted for a minimum of 10 minutes. Pulsed light (I_0) was used for two-photon excitation at 730 nm for more than 75 seconds during which TPEF was recorded continuously. Additional visual stimulation (ΔI) was delivered approximately 37 seconds after the onset of the two-photon excitation light and the duration of the stimulus was varied for different experiments. For all experiments described here, variable amounts of light were used for incremental stimulation (ΔI), whereas the intensity and the wavelength of the two-photon imaging beam (I_0) was fixed. A summary of the experimental parameters is shown in the Table.

Image Analysis and Processing

Interframe eye motion was corrected by using custom software for reflectance and TPEF videos to produce registered videos as well as averaged images of the photoreceptor mosaic, such as those shown in Figures 1c, 1d. The time course of TPEF was analyzed only for rods, and autofluorescence signals from cones were excluded as follows. Coordinates of the center of cone photoreceptors were manually marked in the images generated from registered videos from the reflectance channel using custom MATLAB (MathWorks, Inc., Natick, MA, USA) scripts. Using these coordinates, binary circular masks were created to reject TPEF from cones of each frame for TPEF videos recorded from fluorescence channel. Additionally, those areas within the field of view that had poor image quality or shadows of blood vessels were excluded from subsequent analysis. More details of this aspect of the method can be found in a previous publication.[24]

For analysis, each video was subdivided into two parts: prestimulus and poststimulus, and curve fitting was carried out using custom scripts in MATLAB.

Investigative Ophthalmology & Visual Science

1. Prestimulus data: Single-exponential functions of the form $f(t) = ae^{-k_0 t} + c$ were fit to the time-varying TPEF in the prestimulus phase. Baseline fluorescence levels (F_0) at equilibrium were also estimated from these fits. Although an exponential function was used in our analysis of the prestimulus phase, a more rigorous and physically realistic description of the time-varying concentration of retinol under steady-state illumination has been provided in the Appendix.
2. Poststimulus data: Poststimulus data was identified to be that segment of the measurement that was recorded immediately following the delivery of the stimulus for a period of approximately 50 seconds and its analysis was carried out in multiple steps:
   i) The poststimulus data were fit with double exponential functions of the form $f(t) = a(e^{-k_2 t} - e^{-k_1 t}) + c$ as described in the Appendix using a constrained least-squares fitting approach. This approach requires the user to supply an initial estimate of the fit parameters (a, c, k_1, and k_2 in this case) before fitting the data set as well as the lower and upper bounds for the parameter search space. Values for the upper bound for rate constants k_1 and k_2 were set based on the known temporal sampling of the imaging system, and the initial estimates for k_2 were based on single-exponential fits of the poststimulus data. Errors in the fitting process were estimated through Jacobian analysis.
   ii) The maximum value attained by the double exponential fit was then used to determine the instantaneous fractional increase in TPEF ($\Delta F/F_0$) in response to incremental stimulation ($\Delta I/I_0$).
   iii) In addition to determining the rate constants for retinol removal as described above, the initial rate of retinol removal $\left(R_i = \frac{d}{dt}F\right)$ immediately after stimulation was also estimated by fitting a straight line to the initial 12 seconds of poststimulus TPEF data. This analysis was carried out to assess the order of the reaction, by examining the dependence of the rate of reaction (in this case, the clearance of retinol) as a function of substrate available (in this case, retinol produced due to bleach or ΔF). It is well known that for a first-order reaction, the relationship between the rate of reaction and substrate concentration is expected to be linear, whereas for rate-limited reactions, it can be hyperbolic.

Results

Two-Photon Excited Fluorescence Responses After Incremental Bleach

The time courses of TPEF were recorded under the conditions described in the Methods section, and are shown in Figure 2. As reported previously, with more than 10 minutes of dark adaptation before imaging, TPEF increased after the onset of imaging light. When incremental stimulation was delivered (green bar in each panel), there was a rapid rise in measured TPEF immediately after stimulation. After peaking, TPEF decreased gradually over the duration of the time that it was recorded after stimulation. The rate of increase was too rapid to measure given the limits of our data acquisition rate and signal sensitivity and has not been reported.

Visual inspection of the plots in Figure 2 highlights two key aspects. First, the increase in mean TPEF (ΔF) after fluorescence is related to the intensity of incremental stimulation (ΔI); that is, when more light is delivered to the retina, then more TPEF is measured. Second, the rate at which TPEF decreases after the delivery of stimulus (k_2) is also related to the strength of the stimulus. Quantitative assessment of these parameters is described in subsequent sections.

Two-Photon Excited Fluorescence and Rhodopsin Bleaching

The fractional increase in TPEF ($\Delta F/F_0$) was estimated for varying intensities of light (ΔI) used for incremental visual stimulation. The dependence of $\Delta F/F_0$ on stimulus strength is plotted in Figure 3a (red markers). The increase in fractional TPEF increased somewhat linearly for ΔI values ranging from 6.5 to 7.0 log scotopic troland seconds (td-s). For higher light intensities, the fractional increase in TPEF appeared to become saturated with increasing intensity. The data shown in Figure 3a were fit with an exponential saturation function $\left(1 - e^{-\frac{\Delta I}{I_s}}\right)$. The saturation parameter I_s was estimated to be 6.88 ± 5.50 log scotopic troland.

For the light levels used for two-photon imaging at 730 nm in these experiments, stimulation from the imaging beam (background light) is expected to bleach less than 10% of the available visual pigment in rods (with continual regeneration). The fraction of rod pigment that is expected to be depleted due to incremental bleaches is also plotted in Figure 3a (green markers). These calculations show that photopigment depletion in rods due to stimulation intensities ranging from 6.3 to 7.8 log scotopic td-s follows a trend that is very similar to our experimental estimates of $\Delta F/F_0$. The slight offset between the green and red markers in Figure 3a is likely due to the steady stimulation from the background light. The correspondence between theoretically estimated pigment depletion and the normalized fractional increase in TPEF is highlighted in Figure 3b. For data integrated over all rods during 1 second of acquisition, the signal-to-noise ratio (SNR) was calculated to be 10.9.

Analysis of Decline of TPEF After Incremental Bleach

The rate of TPEF decline after stimulation (k_2) was estimated for various incremental stimulation intensities (ΔI), by fitting exponential decay functions to the poststimulus data. The exponential decay rate constant was found to be dependent on the intensity of incremental stimulus applied, as shown in Figure 4a. An exponential saturation function was used to fit the data shown in Figure 4a, and the saturation parameter I_s was estimated to be 6.78 ± 5.7 log scotopic td-s.

The initial rate of TPEF decline (R_i) was also estimated by fitting straight lines to the initial 12 seconds of data acquired after bleach. These estimates are shown in a scatter plot as a function of initial $\Delta F/F_0$ recorded after bleach in Figure 4b for the same cases shown in Figure 4a. The initial slopes estimated through straight line fits were lower than the values obtained by exponential fits. Moreover, initial slope estimates were found to be weakly dependent on the initial $\Delta F/F_0$ estimated immediately after incremental stimulation.

Discussion

This study demonstrates a simplified method for quantifying time-varying TPEF signals from the living animal eye. Through analytical calculations, we determined that with the application of a brief flash, the rate of all-*trans*-retinol formation and clearance can be directly estimated through simple curve fitting, even in the presence of continual illumination by the two-photon imaging light (see Appendix). This analytical insight has led to the development of a modified experimental

Investigative Ophthalmology & Visual Science

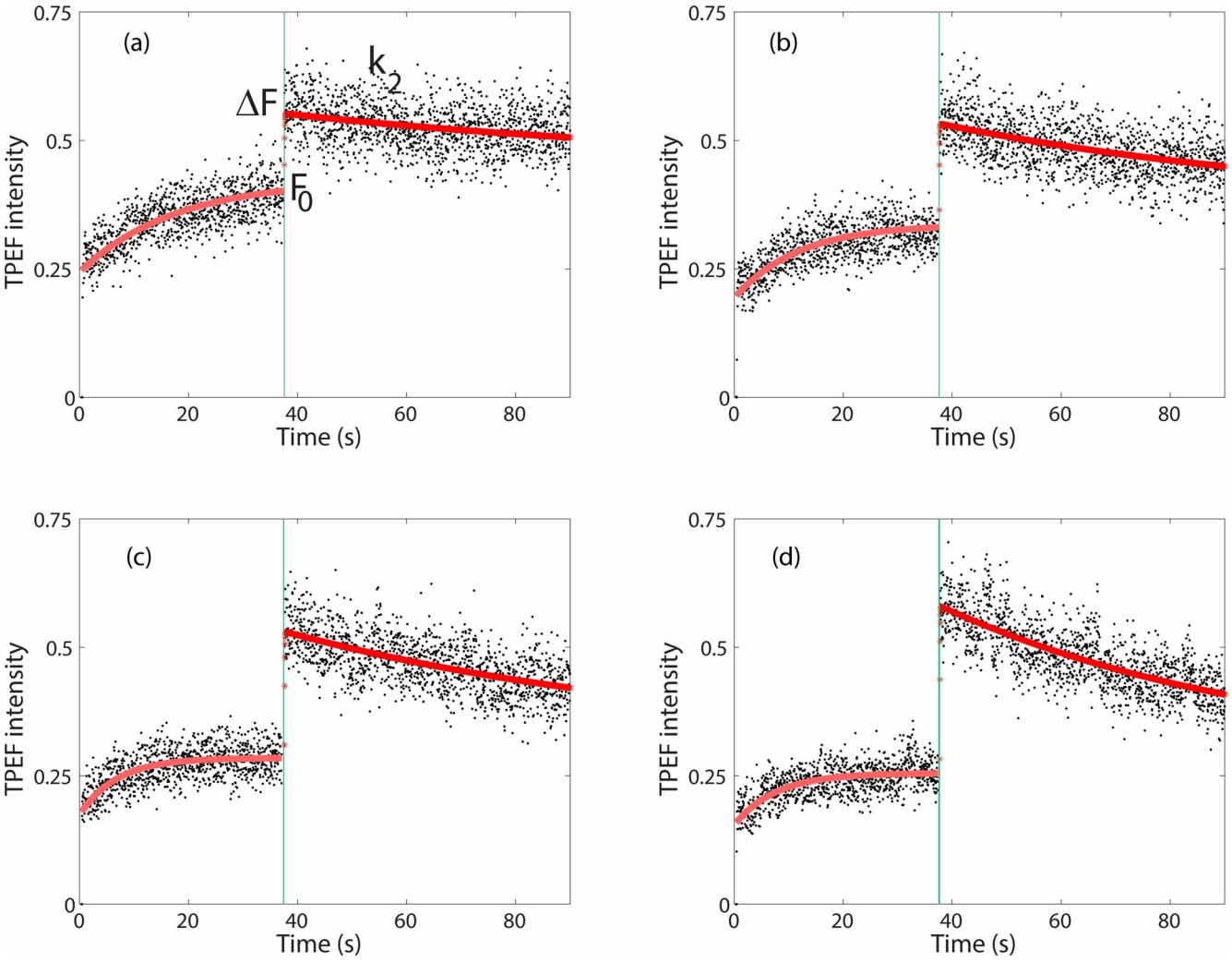

Figure 2. Time course of TPEF from rods under conditions described in the Methods section, Imaging Protocol, are shown here. The *black dots* represent raw data, the *red curves* are exponential fits, and the *green bars* depict the time and duration of the incremental stimulus. Four different conditions are shown here. For all these conditions, the baseline stimulation from the two-photon imaging laser was $I_B = 3.3$ log scotopic troland, corresponding to 3.5 mW of light delivered over a $1.3° \times 1.1°$ field of view. The intensity of the incremental stimulation in log scotopic td-s was 6.37 for (**a**), 6.58 for (**b**), 6.79 for (**c**), and 7.35 for (**d**). The duration of the stimulus was 0.07 second for the cases (**a**), (**b**), and (**c**), and 0.175 second for case (**d**).

protocol that has enabled the investigation of retinol formation and clearance.

Retinol Formation in Rods: An Indirect Measure of Rhodopsin Bleaching

Absorption of light by rhodopsin isomerizes the chromophore from 11-*cis*-retinal to the all-*trans*-retinal configuration. This photoactivation leads to the formation of activated forms of rhodopsin that initiate the phototransduction cascade and release of all-*trans*-retinal. Subsequently, reduction of all-*trans*-retinal by retinol dehydrogenase (RDH8) or other variants in the presence of reduced forms of nicotinamide adenine dinucleotide and nicotinamide adenine dinucleotide phosphate (collectively referred to as NAD(P)H) leads to the formation of all-*trans*-retinol[4,35] and failure of this process can lead to vision impairment.[21,36]

Through the deployment of our modified imaging protocol, we have been able to quantify the amount of retinol generated, $\Delta F/F_0$, as a consequence of photopigment depletion due to brief, incremental stimulation, ΔI. We have observed a dependence of $\Delta F/F_0$ on ΔI and by fitting the data with an exponential saturation function and we extracted a saturation parameter that is equivalent to photosensitivity. Our reported value of photosensitivity estimated through two-photon imaging is 6.88 ± 5.50 log scotopic td-s, which closely agrees with photosensitivity values measured in human subjects.[7–10] Previous studies have used rhodopsin densitometry to measure photopigment depletion after bleach, but our results show that TPEF imaging also can be used to estimate the bleaching of rod photopigment in the living eye as a substitute for rhodopsin densitometry. Because rhodopsin densitometry measurements can be complicated by unknown sources of light scatter,[13,14] the equivalence between TPEF imaging and densitometry provides a simpler and faster alternative. If TPEF imaging was limited by the photon noise, then the SNR can be estimated from experimental data.[37] Based on an SNR of 10.9, the smallest change in TPEF that can be measured reliably (experimental sensitivity) was 9.1%. This is directly related to the smallest change in pigment depletion that can be estimated from such experiments. Given the challenges associated with determining the sources of scattered light, two-photon imaging

Investigative Ophthalmology & Visual Science

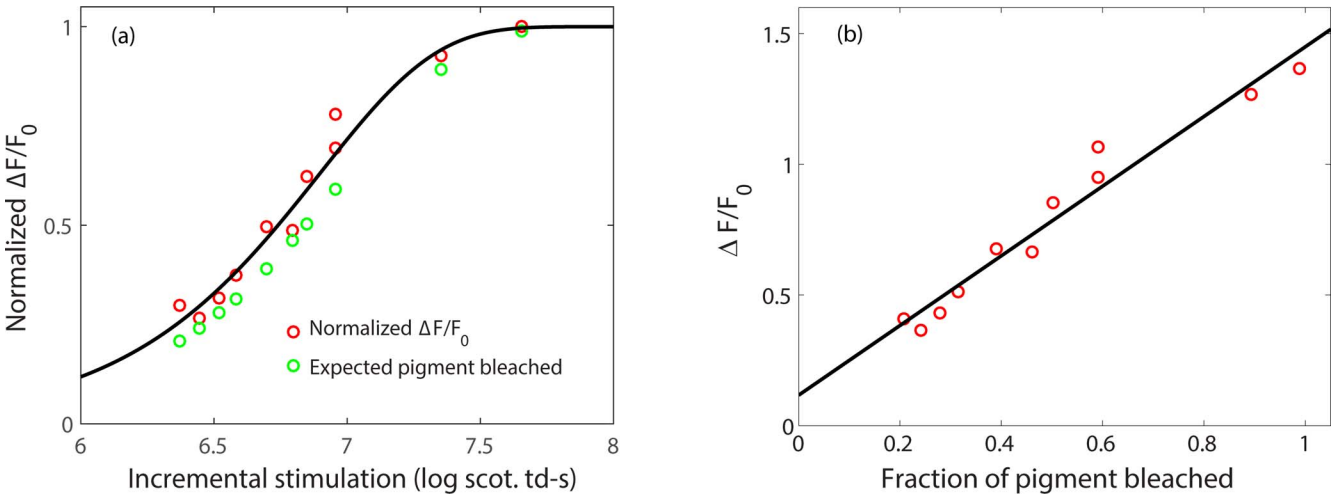

Figure 3. Fractional change in TPEF plotted as a function of intensity of incremental stimulation delivered to the retina measured while the retina was exposed to background illumination $I_B = 3.3$ log scotopic troland. Results shown here are from one animal. Experimental data are plotted with *red markers* and were normalized to the maximum fractional change measured. The fraction of rhodopsin pigment bleached as a consequence of the brief flashes delivered to the retina was calculated by using the photosensitivity parameter ($\sigma = 1e\text{-}7$ scotopic td-s) as reported elsewhere,[8–11] and the results are plotted for reference on the same scale using *green markers*. The experimental data were fit by using an exponential saturation function and are plotted as the *black solid curve* for the best-fit parameter ($R^2 = 0.97$). (**b**) Two-photon excited fluorescence is plotted as a function of the expected fractional pigment bleached depicting the equivalence between fractional TPEF and pigment density. Units on the *x*-axis correspond to 0% to 100% of pigment bleached but are scaled from 0 to 1. The data are fit with a straight line, $y = 1.3331^{*}x + 0.1166$ ($R^2 = 0.955$).

can be a more reliable measure of visual pigment depletion than densitometry, and also can be used to monitor mutational defects in the ABCA4 or RDH pathways through which all-*trans*-retinol is generated. Moreover, reduction of all-*trans*-retinal to all-*trans*-retinol requires NADPH, and delivery of brief, strong flashes of light can possibly push this metabolic capacity to the limit that could potentially be monitored in this manner.

Nevertheless, there are a few aspects related to retinol formation that we have been unable to measure in this study. One of the goals was to estimate the rate constant for retinol formation (k_1) after a brief flash, as described in the Appendix. The data acquisition rate for our imaging apparatus was 26.7 Hz, which is related to the shortest temporal event that can be measured through these experiments. However, as can be seen in Figure 2, in vivo responses from rods were monotonic. This suggests that the temporal resolution was inadequate to measure the rate constant for retinol generation (k_1) and therefore those estimates have not been reported. Improvements in signal detection to boost SNR along with faster scan speeds and frame rates could enable such measurements in the future.

Kinetics of Retinol Clearance From Rods

All-*trans*-retinol is generated within photoreceptor outer segments after reduction of all-*trans*-retinal, and it is then transported across the cell membrane to the RPE.[38] Tracking

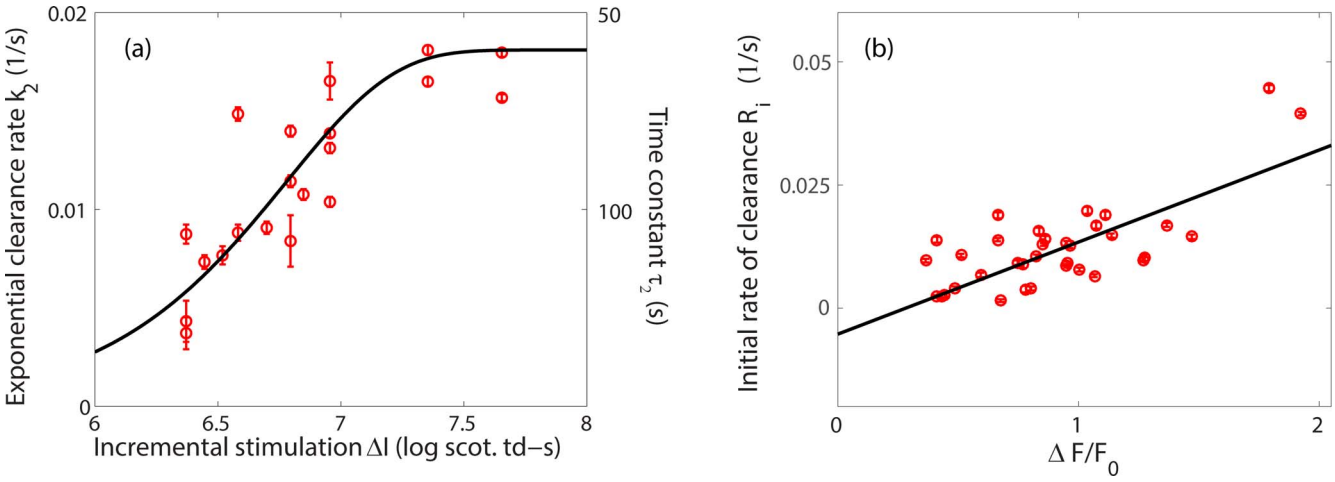

Figure 4. Variation of rate of clearance of retinol with stimulation and initial concentration is depicted in these plots. Results shown are from all three animals. (**a**) Rate constants of TPEF decay, estimated with an exponential fit (first-order kinetics) are plotted as a function of the strength of incremental bleach delivered to the retina. The corresponding time constants are shown on the secondary ordinate axis on the right. The curve in *black* is an exponential saturation fit to the data ($R^2 = 0.70$). (**b**) Initial rate of retinol clearance scaled by the baseline fluorescence $R_i = \frac{1}{F_0}\frac{d}{dt}(F)$ has been plotted against the initial $\Delta F/F_0$ values, measured immediately after stimulus delivery. The data were fit with a straight line, $y = 0.0187x - 0.0053$ ($R^2 = 0.6421$).

Investigative Ophthalmology & Visual Science

the clearance kinetics of all-*trans*-retinol is valuable for studying the health of the photoreceptor-RPE complex in the living eye. However, the biochemical framework for understanding the mechanism of all-*trans*-retinol clearance is complicated and not yet fully understood. The purported role of proteins that can bind to retinoids in protecting and transporting all-*trans*-retinol from the outer segment to the RPE has been the subject of considerable debate.[4,39] Free retinol is toxic and prone to degradation in aqueous solutions, and some retinoid-binding proteins have been shown to protect retinol from decomposition.[40] The mechanism of transport of all-*trans*-retinol from photoreceptors to RPE has been investigated in various studies that have suggested that the interphotoreceptor retinoid-binding protein (IRBP) might be responsible for retinol clearance in vivo[41–44] even though its absence does not affect the rate of photopigment regeneration.[45,46] Retinol clearance could also be mediated by retinoid-binding protein (RPB) or albumin present in the interphotoreceptor matrix.[47,48] Moreover, some reports have shown that the transport of retinol could be mediated by vesicles and liposomes, implying that RPB might serve only as a protective extracellular buffer.[49,50]

In this study, we measured the rate of clearance of retinol as a function of the intensity of a brief incremental stimulus delivered to the eye. Previous studies have assumed that retinol clearance is a first-order process,[27,50,51] and we also restricted our preliminary analysis of retinol clearance to first-order kinetics. In Figure 4b, the initial rate of reaction (R_i), scaled by baseline fluorescence ($1/F_0$) has been plotted against substrate concentration, which is $\Delta F/F_0$ right after stimulation in this case. Although the data are scattered and the R^2 value is low, this plot suggests that there is a weak linear dependence between rate of reaction and substrate concentration right after bleach. This suggests the presence of first-order kinetics. However, the data plotted in Figure 4a suggest that the situation is more complex. The rate constant for retinol clearance was observed to be greater when more intense stimulation was delivered and became saturated for the highest light intensities used for stimulation. Based on the data shown in Figure 3, the saturation behavior is expected if the TPEF signal arising from all-*trans*-retinol is related to rhodopsin bleaching: clearly, for light exposures that completely bleach rhodopsin, the quantity of retinol initially formed will be a constant, and so the rate of removal must also be a constant.

These observations bring into question the role of enzyme kinetics during retinol removal. Retinoid-binding protein, IRBP, and albumin are different types of binding proteins present in abundance in the interphotoreceptor matrix,[4,39] and despite the lack of conclusive evidence, their participation in all-*trans*-retinol clearance could be likely. Moreover, the binding affinity of IRBP for all-*trans*-retinol is known to increase with light adaptation and is approximately five times greater in light than in dark.[52] Here, we found that the rate constant for retinol clearance increases with light stimulation. If IRBP is involved in the clearance of retinol, then the dependence of the rate of clearance on light intensity could be related to the observed changes in the affinity of IRBP for all-*trans*-retinol with light. However, this interpretation is speculative and more experiments are needed to clarify the role of IRBP in the primate eye. Although the findings reported here do not necessarily resolve the mystery behind how retinol is cleared from outer segments, they do not discard the proposition that more complex kinetic schemes could be involved.

Outlook for Implementation in Humans

In our previous study, we measured the rate of retinol clearance after a bleach during dark adaptation[24]; however, in this report, retinol clearance was estimated in the presence of steady-state stimulation from the imaging beam. The protocol described here is more practical than the previous approach for various reasons. First, the proposed methods are more reliable. The previous approach relied on extrapolation of the initial fluorescence trace to generate an intercept value and the kinetics were estimated by curve fitting the initial intercept estimated from 6 to 10 videos acquired over several hours from repeated exposure. By comparison, in the method described in this report, retinol clearance was estimated immediately after bleach by tracking TPEF for more than 45 seconds at a 26.7 Hz frame rate (~1500 data points). Second, the technique proposed in this report is safer than our previous approach. In the previous protocol, the same retinal location had to be exposed to pulsed light multiple times for approximately 2 minutes each time over a 3-hour duration to generate the retinol clearance trace, whereas in the protocol described here, retinol clearance can be estimated by using just one exposure of 90 seconds' duration at 730 nm and a brief flash at 561 nm. Third, the method described in this report is faster. Retinol clearance can be tracked by using one video of approximately 90-seconds' duration, unlike the previous approach wherein multiple videos had to be acquired at the same retinal location over several hours.

By recording longer-duration videos, better fits could have been obtained for k_2 during the decline of TPEF, but due to concerns about altering the physiological state of the retina because of overexposure, we recorded videos of just approximately 90 seconds' duration. Consequently, it is unknown if TPEF would eventually return to prestimulus baseline levels, although the responses were always observed to be monotonic. Nevertheless, it is unclear if an exposure of 90 seconds is totally harmless. Even though we did not observe any retinal damage with the methods available, light safety is a major concern because TPEF imaging necessitates exposing the retina to ultrashort pulses. Unfortunately, safety limits have not yet been rigorously investigated and established for pulses of pulse-width less than 100 fs.[53] An ongoing study is evaluating the safety of using this imaging technique in humans and this will be crucial to verify the efficacy of two-photon imaging in humans.

Conclusions

This work has demonstrated a framework for rapidly extracting physiologically relevant information through TPEF imaging of all-*trans*-retinol in rods. We have shown that in vivo two-photon ophthalmoscopy can be used to estimate photopigment depletion through all-*trans*-retinol formation. We have used this technique to estimate the photosensitivity of rhodopsin in the macaque eye. Moreover, we have estimated the kinetics of retinol clearance from rod photoreceptors in the presence of background illumination from the imaging beam. Although first-order kinetics models might be insufficient to completely describe the data, they do provide a convenient approximation for retinol clearance pathways in the living eye, even though a comprehensive biochemical framework for understanding the mechanism of all-*trans*-retinol clearance in primates is lacking. In the future, the analytical model detailed in the Appendix and the experimental protocols described here could be used to rapidly assess visual cycle defects in normal and diseased primate populations and evaluate the efficacies of various therapies for retinal diseases.

Investigative Ophthalmology & Visual Science

Appendix

In vivo two-photon imaging at 730 nm imposes the condition that the retina was subjected to steady-state stimulation during recording, as shown previously.[24,29] To understand this time-varying TPEF, we developed an analytical scheme, similar to theoretical models proposed previously by other investigators.[27,54,55] For simplicity, several assumptions were made:

1. All-*trans*-retinol was considered to be the dominant source of time-varying TPEF.
2. The modulatory effect of screening pigments on TPEF was considered negligible.
3. All reactions were believed to follow first-order kinetics.
4. The visual cycle was considered a closed-loop unidirectional subsystem.

Figure 1a describes those components of the visual cycle that are involved in the formation and clearance of all-*trans*-retinol. The kinetics of rhodopsin during steady-state illumination have been described previously.[55] The rate equations for the subsequent generation of retinal and retinol were assumed to follow first-order kinetics, similar to previous reports.[9,54] However, we acknowledge that the validity of first-order kinetics for retinol formation is contingent on the availability of NAD(P)H for reduction of all-*trans*-retinal,[56] something that is expected to be true for weak bleaches. However, this assumption could potentially break down for strong bleaches.[51] Figure 1a also depicts retinosomes in the RPE where retinol is sequestered as retinyl esters during the visual cycle.[17]

Rate equations for the system described in Figure 1 during steady-state illumination are given below.

$$\frac{d\,Rh(t)}{dt} = k_3 c(t) Ops(t) - \sigma I_0(t) Rh(t) \tag{1}$$

$$\frac{d\,Ops(t)}{dt} = \sigma I_0(t) Rh(t) - k_3 c(t) Ops(t) \tag{2}$$

$$Rh(t) + Ops(t) = C_0 \qquad \text{Constant} \tag{3}$$

$$\frac{d\,[RAL](t)}{dt} = \sigma I_0(t) Rh(t) - k_1 [RAL](t) \qquad \text{(All-}trans\text{-retinal)} \tag{4}$$

$$\frac{d\,[ROL](t)}{dt} = k_1 [RAL](t) - k_2 [ROL](t) \qquad \text{(All-}trans\text{-retinol)} \tag{5}$$

$$\frac{d\,c(t)}{dt} = k_2 [ROL](t) - k_3 c(t) Ops(t) \qquad \text{(11-}cis\text{-retinal)} \tag{6}$$

$$\frac{d\,Rh(t)}{dt} = v(1 + K_m)\frac{1 - Rh(t)}{1 + K_m - Rh(t)} - \sigma I_0(t) Rh(t) \tag{7}$$

where

$Rh(t)$, quantity of unbleached rhodopsin as a function of time
$Ops(t)$, quantity of bleached opsin as a function of time
$[RAL](t)$, quantity of all-*trans*-retinal
$[ROL](t)$, quantity of all-*trans*-retinol
$c(t)$, quantity of 11-*cis*-retinal
I_0, intensity of constant incident light in trolands
σ, photosensitivity of photopigment trolands^{-1} s^{-1}
k_1, k_2, and k_3, rate constants shown in Figure 1 in s^{-1}
C_o, physical constant
v and K_m, parameters described by the MLP equation[55]
$A(s)$, Laplace transform of $[RAL](t)$
$B(s)$, Laplace transform of $[ROL](t)$
$C(s)$, Laplace transform of $c(t)$
$R(s)$, Laplace transform of $Rh(t)$

Application of Laplace transform gives us the following relationships, during steady-state constant illumination ($I = I_0$), from equations 3 and 4:

$$A(s) = \frac{\sigma I_0 R(s) + [RAL(0)]}{s + k_1} \qquad \text{(All-}trans\text{-retinal)} \tag{8}$$

$$B(s) = \frac{k_1 A(s) + [ROL(0)]}{s + k_2} \qquad \text{(All-}trans\text{-retinol)} \tag{9}$$

and consequently,

$$B(s) = \frac{[ROL(0)]}{(s + k_2)} + \frac{k_1 [RAL(0)]}{(s + k_1)(s + k_2)} + \frac{k_1 \sigma I_0}{(s + k_1)(s + k_2)} R(s) \tag{10}$$

After inverse Laplace transform, this becomes

$$[ROL(t)] = [ROL(0)] e^{-k_2 t} + \frac{k_1 [RAL(0)]}{(k_2 - k_1)}\left[e^{-k_1 t} - e^{-k_2 t}\right] + \frac{k_1 \sigma I_0}{(k_2 - k_1)}\left\{\int_0^t Rh(t - \tau)\left[e^{-k_1 \tau} - e^{-k_2 \tau}\right] d\tau\right\} \tag{11}$$

Mahroo and Lamb[55] provided an expression for rhodopsin during steady-state illumination that is a solution of equation 7 (equation A12 in their article, shown here).

$$t = \left[\left(\frac{a}{d}\right) ln \frac{(d + 2LP - b)(d - 2LP_0 + b)}{(d + 2LP_0 - b)(d - 2LP + b)} - ln \frac{LP^2 + bP + (1 + K_m)v}{LP_0^2 + bP_0 + (1 + K_m)v}\right] \Big/ 2L, \tag{12}$$

where a, b, d, and L are parameters that are related to σ, I_0, K_m, and v.

Special Case: Incremental Transient Stimulus Delivered During Steady State

In this case, the light incident on the retina at $t = t_0$ is described by the following function:

$$I = I_0 + \Delta I \delta(t - t_0) \tag{13}$$

Substituting this in the rate equations above and taking Laplace transform of all-*trans*-retinal gives us

$$A(s) = \frac{\sigma I_0 R(s) + [RAL(0)]}{s + k_1} + \frac{\sigma \Delta I Rh(t_0)}{(s + k_1)} e^{-st_0} \qquad \text{(all-}trans\text{-retinal)} \tag{14}$$

And consequently, the expression for all-*trans*-retinol becomes

$$B(s) = \frac{[ROL(0)]}{(s+k_2)} + \frac{k_1[RAL(0)]}{(s+k_1)(s+k_2)} + \frac{k_1\sigma I_0}{(s+k_1)(s+k_2)}R(s) + \frac{k_1\sigma\Delta IRh(t_0)}{(s+k_1)(s+k_2)}e^{-st_0} \quad \text{(all-}trans\text{-retinol)} \quad (15)$$

After inverse Laplace transform this can be written as

$$[ROL(t)] = [ROL(0)]e^{-k_2t} + \frac{k_1[RAL(0)]}{(k_2-k_1)}\left[e^{-k_1t} - e^{-k_2t}\right] + \frac{k_1\sigma I_0}{(k_2-k_1)}\left\{\int_0^t Rh(t-\tau)\left[e^{-k_1\tau} - e^{-k_2\tau}\right]d\tau\right\} + H(t-t_0)\frac{k_1\sigma\Delta IRh(t_0)}{(k_2-k_1)}\left[e^{-k_1(t-t_0)} - e^{-k_2(t-t_0)}\right], \quad (16)$$

where $H(t)$ is the Heaviside step function. We have previously reported that after a sufficient period, TPEF plateaus and stabilizes. If this incremental stimulus is delivered when retinol production and clearance have plateaued ($t \rightarrow t_p$), then we can rewrite the above expression as

$$[ROL(t)] = \left[ROL(t_p)\right] + H(t-t_0)\frac{k_1\sigma\Delta IRh(t_0)}{(k_2-k_1)}\left[e^{-k_1(t-t_0)} - e^{-k_2(t-t_0)}\right]. \quad (17)$$

Thus, under the first-order approximation, the retinol response after brief flash can be modeled as a double exponential function, similar to what has previously been done by other investigators.[27,51,54] The experimental implementation of this special case is described in the Methods section, Imaging Protocol, and the subsequent data analysis required to fit TPEF data is described in the Methods section, Image Analysis and Processing.

Acknowledgments

The authors thank Ted Tweitmeyer, Keith Parkins, Lee Anne Schery, Tracy Bubel, Jesse Schallek, Ethan Rossi, Sarah Walters, James Feeks, and Jie Zhang for their contributions in enabling some of the work reported here.

The image acquisition software and firmware were developed by Qiang Yang and the adaptive optics control software was developed by Alfredo Dubra and Kamran Ahmad at the University of Rochester. Custom image registration software DeMotion was developed by Alfredo Dubra and Zachary Harvey with funding from Research to Prevent Blindness (New York, NY, USA) and the National Institutes of Health (Bethesda, MD, USA) through Grants BRP-EY014375 and 5 K23 EY016700. The stereotaxic cart design is courtesy of the US Air Force, and was constructed with modifications by Martin Gira and Mark Ditz at the University of Rochester. Reflectance image analysis software was adopted from Ethan Rossi and Kaccie Li and was developed at the University of California, Berkeley. Animals were handled by Lee Anne Schery, Amber Walker, or Louis DiVincenti before and during experimentation.

Supported in part by an unrestricted grant to the Flaum Eye Institute at the University of Rochester from Research to Prevent Blindness Grants R44 AG043645, R01 EY022371, and P30 EY001319 and the Arnold and Mabel Beckman Foundation. K.P. is CSO of Polgenix, Inc., and John H. Hord Professor of Pharmacology.

Disclosure: **R. Sharma**, Polgenix, Inc. (F), P; **C. Schwarz**, Polgenix, Inc. (F); **J.J. Hunter**, Polgenix, Inc. (F), P; **G. Palczewska**, Polgenix, Inc. (E); **K. Palczewski**, Polgenix, Inc. (C), P; **D.R. Williams**, Canon, Inc. (R), Polgenix, Inc. (F), P

References

1. Wald G. Cartenoids and the visual cycle. *J Gen Physiol*. 1935; 19:351–371.
2. Strauß O. Transport mechanisms of the retinal pigment epithelium to maintain of visual function. *Heat Mass Transf*. 2014;50:303.
3. Kiser PD, Golczak M, Palczewski K. Chemistry of the retinoid (visual) cycle. *Chem Rev*. 2014;114:194–232.
4. McBee JK, Palczewski K, Baehr W, Pepperberg DR. Confronting complexity: the interlink of phototransduction and retinoid metabolism in the vertebrate retina. *Prog Retin Eye Res*. 2001;20:469–529.
5. Baehr W, Wu SM, Bird AC, Palczewski K. The retinoid cycle and retina disease. *Vision Res*. 2003;43:2957–2958.
6. Lamb TD, Pugh EN. Dark adaptation and the retinoid cycle of vision. *Prog Retin Eye Res*. 2004;23:307–380.
7. Rushton WA. The difference spectrum and the photosensitivity of rhodopsin in the living human eye. *J Physiol*. 1956;134: 11–29.
8. Ripps H, Weale RA. Flash bleaching of rhodopsin in the human retina. *J Physiol*. 1969;200:151–159.
9. Alpern M. Rhodopsin kinetics in the human eye. *J Physiol*. 1971;217:447–471.
10. Morgan JIW, Pugh EN Jr. Scanning laser ophthalmoscope measurement of local fundus reflectance and autofluorescence changes arising from rhodopsin bleaching and regeneration. *Invest Ophthalmol Vis Sci*. 2013;54:2048–2059.
11. Campbell FW, Rushton WAH. Measurement of the scotopic pigment in the living human eye. *J Physiol*. 1955;130:131–147.
12. Ripps H, Weale RA. Rhodopsin regeneration in man. *Nature*. 1969;222:775–777.
13. Grieve K, Roorda A. Intrinsic signals from human cone photoreceptors. *Invest Ophthalmol Vis Sci*. 2008;49:713–719.
14. Masella BD, Hunter JJ, Williams DR. New wrinkles in retinal densitometry. *Invest Ophthalmol Vis Sci*. 2014;55:7525–7534.
15. Denk W, Strickler JH, Webb WW. Two-photon laser scanning fluorescence microscopy. *Science*. 1990;248:73–76.
16. Imanishi Y, Batten ML, Piston DW, Baehr W, Palczewski K. Noninvasive two-photon imaging reveals retinyl ester storage structures in the eye. *J Cell Biol*. 2004;164:373–383.
17. Imanishi Y, Gerke V, Palczewski K. Retinosomes: new insights into intracellular managing of hydrophobic substances in lipid bodies. *J Cell Biol*. 2004;166:447–453.
18. Palczewska G, Maeda T, Imanishi Y, et al. Noninvasive multiphoton fluorescence microscopy resolves retinol and retinal condensation products in mouse eyes. *Nat Med*. 2010; 16:1444–1449.
19. Maeda A, Palczewska G, Golczak M, et al. Two-photon microscopy reveals early rod photoreceptor cell damage in light-exposed mutant mice. *Proc Natl Acad Sci U S A*. 2014; 111:E1428–E1437.
20. Palczewska G, Dong Z, Golczak M, et al. Noninvasive two-photon microscopy imaging of mouse retina and retinal pigment epithelium through the pupil of the eye. *Nat Med*. 2014;20:785–789.
21. Maeda A, Palczewski K. Retinal degeneration in animal models with a defective visual cycle. *Drug Discov Today Dis Models*. 2013;10:e163–e172.
22. Dacey D. Origins of perception: retinal ganglion cell diversity and the creation of parallel visual pathways. In: Gazzaniga MS,

ed. *The Cognitive Neurosciences*. 3rd ed. Cambridge, MA: MIT Press; 2004:281–301.

23. Sharma R, Williams DR, Palczewska G, Palczewski K, Hunter JJ. Two-photon autofluorescence imaging reveals cellular structures throughout the retina of the living primate eye. *Invest Opthalmol Vis Sci*. 2016;57:632.
24. Sharma R, Schwarz C, Williams DR, Palczewska G, Palczewski K, Hunter JJ. In vivo two-photon fluorescence kinetics of primate rods and cones. *Invest Ophthalmol Vis Sci*. 2016;57:647.
25. Hunter JJ, Masella B, Dubra A, et al. Images of photoreceptors in living primate eyes using adaptive optics two-photon ophthalmoscopy. *Biomed Opt Express*. 2011;2:139–148.
26. Chen C, Tsina E, Cornwall MC, Crouch RK, Vijayaraghavan S, Koutalos Y. Reduction of all-*trans* retinal to all-*trans* retinol in the outer segments of frog and mouse rod photoreceptors. *Biophys J*. 2005;88:2278–2287.
27. Chen C, Blakeley LR, Koutalos Y. Formation of all-*trans* retinol after visual pigment bleaching in mouse photoreceptors. *Invest Ophthalmol Vis Sci*. 2009;50:3589–3595.
28. Palczewska G, Golczak M, Williams DR, Hunter JJ, Palczewski K. Endogenous fluorophores enable two-photon imaging of the primate eye. *Invest Ophthalmol Vis Sci*. 2014;55:4438–4447.
29. Palczewska G, Vinberg F, Stremplewski P, et al. Human infrared vision is triggered by two-photon chromophore isomerization. *Proc Natl Acad Sci U S A*. 2014;111:E5445–E5454.
30. Liang J, Williams DR, Miller DT. Supernormal vision and high-resolution retinal imaging through adaptive optics. *J Opt Soc Am A Opt Image Sci Vis*. 1997;14:2884–2892.
31. Roorda A, Romero-Borja F, Donnelly I, Queener H, Hebert T, Campbell M. Adaptive optics scanning laser ophthalmoscopy. *Opt Express*. 2002;10:405–412.
32. Dubra A, Harvey Z. Registration of 2D images from fast scanning ophthalmic instruments. In: Fischer B, Dawant BM, Lorenz C, eds. *Biomedical Image Registration. Lecture Notes in Computer Science*. Berlin: Springer; 2010:60–71.
33. Arathorn DW, Yang Q, Vogel CR, Zhang Y, Tiruveedhula P, Roorda A. Retinally stabilized cone-targeted stimulus delivery. *Opt Express*. 2007;15:13731–13744.
34. Yin L, Masella B, Dalkara D, et al. imaging light responses of foveal ganglion cells in the living macaque eye. *J Neurosci*. 2014;34:6596–6605.
35. Kiser PD, Golczak M, Maeda A, Palczewski K. Key enzymes of the retinoid (visual) cycle in vertebrate retina. *Biochim Biophys Acta*. 2012;1821:137–151.
36. Travis GH, Golczak M, Moise AR, Palczewski K. Diseases caused by defects in the visual cycle: retinoids as potential therapeutic agents. *Annu Rev Pharmacol Toxicol*. 2007;47:469–512.
37. Dobbins JT III. Image quality metrics for digital systems. In: Van Metter RL, Beutel J, Kundel HL, eds. *Handbook of Medical Imaging, Volume 1. Physics and Psychophysics*. Bellingham, WA: SPIE; 2000:161–222.
38. Dowling JE. Chemistry of visual adaptation in the rat. *Nature*. 1960;188:114–118.
39. Ripps H. The rhodopsin cycle: a twist in the tale. *Prog Brain Res*. 2001;131:335–350.
40. Crouch RK, Hazard ES, Lind T, Wiggert B, Chader G, Corson DW. Interphotoreceptor retinoid-binding protein and alpha-tocopherol preserve the isomeric and oxidation state of retinol. *Photochem Photobiol*. 1992;56:251–255.
41. Okajima TI, Pepperberg DR, Ripps H, Wiggert B, Chader GJ. Interphotoreceptor retinoid-binding protein: role in delivery of retinol to the pigment epithelium. *Exp Eye Res*. 1989;49:629–644.
42. Pepperberg DR, Okajima TL, Wiggert B, Ripps H, Crouch RK, Chader GJ. Interphotoreceptor retinoid-binding protein (IRBP). Molecular biology and physiological role in the visual cycle of rhodopsin. *Mol Neurobiol*. 1993;7:61–85.
43. Qtaishat NM, Wiggert B, Pepperberg DR. Interphotoreceptor retinoid-binding protein (IRBP) promotes the release of all-*trans* retinol from the isolated retina following rhodopsin bleaching illumination. *Exp Eye Res*. 2005;81:455–463.
44. Wu Q, Blakeley LR, Cornwall MC, Crouch RK, Wiggert BN, Koutalos Y. Interphotoreceptor retinoid-binding protein is the physiologically relevant carrier that removes retinol from rod photoreceptor outer segments. *Biochemistry*. 2007;46:8669–8679.
45. Palczewski K, Van Hooser JP, Garwin GG, Chen J, Liou GI, Saari JC. Kinetics of visual pigment regeneration in excised mouse eyes and in mice with a targeted disruption of the gene encoding interphotoreceptor retinoid-binding protein or arrestin. *Biochemistry*. 1999;38:12012–12019.
46. Ripps H, Peachey NS, Xu X, Nozell SE, Smith SB, Liou GI. The rhodopsin cycle is preserved in IRBP "knockout" mice despite abnormalities in retinal structure and function. *Vis Neurosci*. 2000;17:97–105.
47. Quadro L, Blaner WS, Salchow DJ, et al. Impaired retinal function and vitamin A availability in mice lacking retinol-binding protein. *EMBO J*. 1999;18:4633–4644.
48. Adler AJ, Edwards RB. Human interphotoreceptor matrix contains serum albumin and retinol-binding protein. *Exp Eye Res*. 2000;70:227–234.
49. Fex G, Johannesson G. Retinol transfer across and between phospholipid bilayer membranes. *Biochim Biophys Acta*. 1988;944:249–255.
50. Ho MT, Massey JB, Pownall HJ, Anderson RE, Hollyfield JG. Mechanism of vitamin A movement between rod outer segments, interphotoreceptor retinoid-binding protein, and liposomes. *J Biol Chem*. 1989;264:928–935.
51. Ala-Laurila P, Kolesnikov AV, Crouch RK, et al. Visual cycle: dependence of retinol production and removal on photoproduct decay and cell morphology. *J Gen Physiol*. 2006;128:153–169.
52. Adler AJ, Spencer SA. Effect of light on endogenous ligands carried by interphotoreceptor retinoid-binding protein. *Exp Eye Res*. 1991;53:337–346.
53. ANSI. *American National Standard for Safe Use of Lasers ANSI Z136.1-2014*. Orlando, FL: Laser Institute of America; 2014.
54. Baumann C, Bender S. Kinetics of rhodopsin bleaching in the isolated human retina. *J Physiol*. 1973;235:761–773.
55. Mahroo O, Lamb T. Recovery of the human photopic electroretinogram after bleaching exposures: estimation of pigment regeneration kinetics. *J Physiol*. 2004;554:417–437.
56. Palczewski K, Jager S, Buczylko J, et al. Rod outer segment retinol dehydrogenase: substrate specificity and role in phototransduction. *Biochemistry*. 1994;33(46):13741–13750.

Investigative Ophthalmology & Visual Science